

Results of some R-D projects on the non-conventional (green) energy

Nguyen Nang Dinh
University of Engineering and Technology
Vietnam National University, Hanoi
144, Xuan Thuy, Cau Giay, Hanoi, Vietnam.
dinhnn@vnu.edu.vn

Abstract. Non-conventional energy or *Green energy* includes Solar, Wind, Sea-waves energy and also Energy-efficient windows are subjects that are being intensively carried-out in University of Engineering and Technology, Vietnam National University (UET-VNU) for further application in Vietnam. In this report we present main research results concerning to solar energy. There are R-D groups of projects in following fields: The first, research and application of how to use solar radiation most efficiently, so called "Energy-Efficient Windows", The second, research and produce of solid-state lighting sources - the most efficiently lighting lamps; and the last, research of new type of solar cells, such as Organic Solar Cells (OSC).

I. Energy-efficient windows

Energy efficient windows are sometimes called "smart windows", consisting of electrochromic (EC) and thermochromic (TC) thin layers which are coated on glass.

1.1. Electrochromic windows

It is well known that EC materials are able to change their optical properties reversibly and persistently by charge insertion/extraction. They can be integrated in multilayer constructions devised for energy efficient windows, information displays, etc. EC-based fenestration is of much current interest and can provide significant energy savings in buildings jointly with a comfortable indoor climate. A conventional EC device incorporates a tungsten oxide thin film separated from another thin film serving as a counter electrode by an ion conductor, and this three-layer stack is embedded between transparent electrical conductors for inserting/extracting the charge [1]. Tungsten oxide darkens under charge insertion, i.e., cathodically. Ideally, the counter electrode should darken under charge extraction, i.e., anodically, and a hydrous nickel oxide film is a particularly good option for devices [2,3]. Another alternative is to have an essentially non-coloring counter electrode. Thinfilms and nanoparticles of TiO_2 can display EC properties, and this material has attracted sporadic interest for almost forty years.

A thorough examination of the scientific literature has identified numerous previous studies on the electrochromism of TiO_2 -based thin films and particle coatings. The latter property is expressed in terms of a coloration efficiency η taken to be the difference in optical density per amount of charge insertion/extraction. Except when otherwise noted, the data pertain to Li^+ exchange. In general η depends on the wavelength λ , but for our purpose it is sufficient to state a value that is typical for the luminous range, i.e., for a value in the 400 to 700 nm interval. We first consider some films made by evaporation [4,5], whose coloration efficiency was found to be small. Sputter deposition has attracted more widespread interest, and TiO_2 -based films have been prepared by RF [6] and DC techniques [7]. Significantly larger values were subsequently found by Kitao et al. [8], who reported $\eta \approx 9 \text{ cm}^2/\text{C}$ for Li^+ exchange and $\eta \approx 14 \text{ cm}^2/\text{C}$ for H^+ exchange. These results are important as a motivation for our present investigation and point at the critical role of the film nanostructure and that in general deposition parameters promoting porosity lead to large coloration efficiency. A similar result, though less detailed, was found in work by Lee [9]. Chemical bath deposition has been used several times to make TiO_2 -based films with EC properties and have yielded different coloration efficiencies from 9 to $25 \text{ cm}^2/\text{C}$. A value as high as $\eta \approx 26 \text{ cm}^2/\text{C}$ was reported by Richardson and Rubin [10]. The studies by Lin et al. and Wang et al. indicate again that annealing and accompanying densification tend to decrease the coloration efficiency. Among

electrochemical methods for making TiO₂-based films we note that anodization as well as cathodic electrodeposition have been used. The very recent work by Lee et al. [11] showed $\eta \approx 16 \text{ cm}^2/\text{C}$ when the anodization conditions were appropriate for making a “mesoporous” structure. Anodization can be used also for preparing nanotubes, and such samples have shown electrochromism both in H⁺ and Li⁺ electrolytes. There are other techniques that are applicable too. Thus a doctor blade technique has been employed recently by our Lab. [12,13] and has given TiO₂ films with $\eta \approx 34 \text{ cm}^2/\text{C}$. We used two thin adhesive tapes (30 μm in thickness) put parallel and 1 cm apart from each other, creating a slot on the FTO-coated glass slide to contain the colloidal solution. A glass slide overcoated with a 0.2 μm thick FTO film having a sheet resistance of 15 $\Omega/$ and a transmittance of 90% was used as a substrate; the useful area that constitutes the sample studied was of 1 cm². A colloidal solution of 15 wt % nanoparticles (15 nm in size) of titanium oxide (Nyacol Products) in water was used. For producing thinner films we added more distilled water to get ca. 5 wt % TiO₂ and a few drops of the liquid surfactance were added. Then the diluted solution was filled in the slot on the FTO electrode and spread along the tapes. The samples were left for drying during 15 min before annealing at 450°C in air for 1h.

The thickness of the films was found to be depending on preparation conditions such as the concentration of solutions and the spread speed. The samples used for further investigation were taken from films chosen with a concentration of 5 wt % TiO₂ in water and a spread speed of 8 mm/s. The bright-field micrographs of the films are shown in Fig. 1a. The thickness of the film was measured from a FE-SEM scanned at a cross section of the film by point-to-point marking technique, as shown in Fig. 1b. The film is well uniform, but some crystallized nanoparticles are a little larger than the initial TiO₂ particles dispersed in water (namely 20 nm in size). The thickness of the films ranges from 500 to 550 nm. In comparison with the nanostructured films prepared by sol-gel method these films are thicker and much more porous. Although the nc-TiO₂ particles are attached to each other tightly, between them there are numerous nanoscale pores which favour the insertion of ions like Li⁺ or Na⁺ into the films, when a polarized potential is applied on the working electrode (nc-TiO₂/FTO). The crystalline structure of the films was confirmed by using an accessory for films with a small angle of the X-ray incident beam. From the XRD analysis, grains size was found to be of ca. 25 nm.

For the TiO₂ films deposited by the sol-gel technique, the time to get a saturated state of coloration was as large as 45 min for a sample size of 1 cm². The nc-TiO₂/FTO was coloured very rapidly for a sample of the same size. The saturated coloration was reached about 5 sec after a negative potential of -1.20 V/SCE was applied to the WE in the 1M LiClO₄ + PC electrolyte. A deep blue colour was observed in the coloration state and a completely transparent bleaching state was obtained after less than 5 sec.

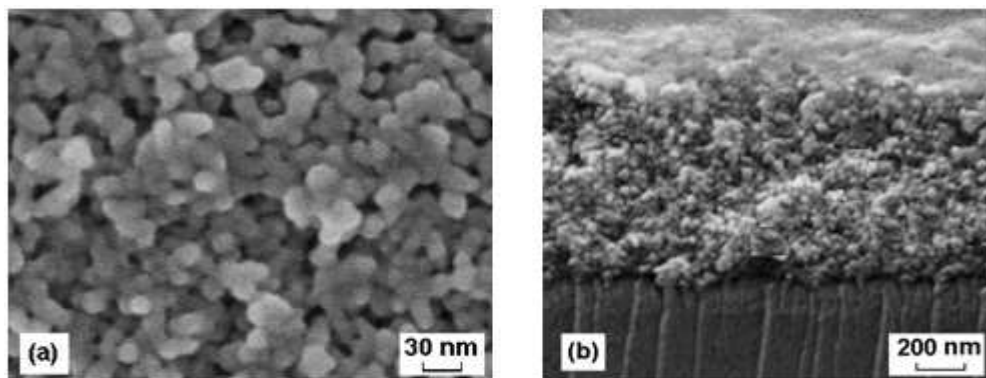


Fig. 1. FE-SEM bright-field micrograph of a doctor-blade deposited TiO₂ film: surface view (a) and cross-section (b). The concentration of the colloidal solution was 5 wt.% TiO₂ in water, and the spread speed was 8 mm/s. The thickness d of the film was about 550 nm.

For a sample with a 550 nm-thick nc-TiO₂ film on FTO-coated glass, the *in situ* transmission spectra, obtained during coloration at a polarized potential of -1.2 V/SCE are given in Fig. 2. The first spectrum (curve 1) is the transmittance in open circuit. The plots denoted by numbers from 2, 3, 4 and 5 and correspond respectively to coloration times of 0.5, 1, 1.5 and 2sec. The curve 6 is of the saturated coloration, the completely bleached state occurred also fast, after approximately 2 sec (curve 7). At $\lambda = 550$ nm (for the best human-eye sensitivity) the transmittance of the open circuit state is as high as 78%, whereas the transmittance of the saturated coloration state is as low as 10% (curves 1 and 6 in Fig. 2).

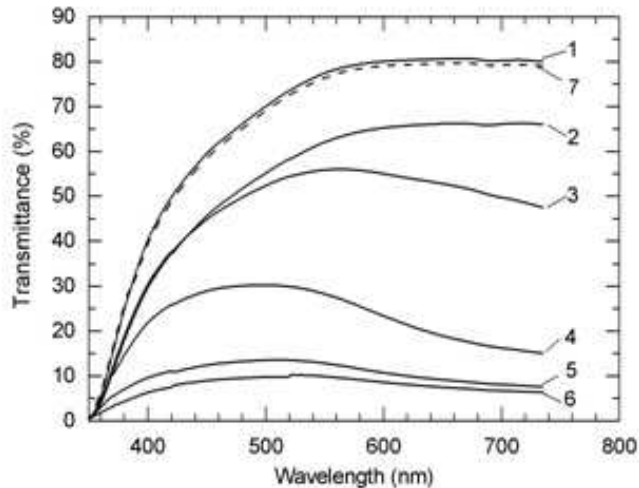


Fig. 2. *In situ* transmission spectra of the TiO₂/FTO colored in 1M LiClO₄ + PC at -1.20 V/SCE versus time. The 1st curve is the transmittance spectra in open circuit; 2, 3, 4 and 5 - the spectra corresponding to respective coloration times of 0.5, 1, 1.5 and 2sec; 6 - saturated coloration state; 7 - completely bleached state.

To evaluate the electrochromic coloration efficiency (η) we used a well-known expression relating the efficiency with the optical density, consequently the transmittances of coloration (T_c) and bleaching states (T_b), and the insertion charge (Q) are as follows:

$$\eta = \frac{\Delta OD}{Q} = \frac{1}{Q} \ln \left(\frac{T_b}{T_c} \right) \quad (1)$$

The λ - η plot for the electrochromic performance is shown in Fig. 8. At a wavelength of 550 nm, $Q = 0.61 \text{ mC} \times \text{cm}^{-2}$, $T_b = 78\%$ and $T_c = 10\%$, the coloration efficiency was determined to be $33.7 \text{ cm}^2 \times \text{C}^{-1}$. The larger is the wavelength, the higher is the coloration efficiency. In the visible range of wavelengths all the values of η found are comparable to those for WO₃ films [14] and much higher than those for TiO₂ films [15] prepared by sol-gel techniques and titanium-lanthanide oxides deposited by magnetron sputtering and coloured in a LiClO₄ + PC solution. By applying a cathodic potential (- 1.20 V/SCE) to FTO, the colour of WE became deep-blue. With the switching of the polarization of the WE to a positive potential, namely + 1.20 V/SCE, the WE returned to its original transmission state.

For the EC-smart windows, nanostructured porous TiO₂ anatase films with a grain size of 20 nm were deposited on transparent conducting FTO electrodes by a doctor-blade method using a colloidal TiO₂ solution. Electrochromic performance of TiO₂/FTO was carried out in 1M LiClO₄ + propylene carbonate and a good reversible coloration and bleaching process was obtained. The response time of the ECD coloration was found to be as small as 2 s and the coloration efficiency could be as high as $33.7 \text{ cm}^2 \times \text{C}^{-1}$. *In situ* transmittance spectra and XRD analysis of the TiO₂/FTO working electrode demonstrated the insertion/extraction of Li⁺ ions into anatase TiO₂. Simultaneous use of chronoamperometry and XRD allowed the

determination of the compound of the saturated coloration state of WE to be $\text{Li}_{0.5}\text{TiO}_2$. The results showed that nanostructured porous TiO_2 films can be comparable in property to WO_3 films. Since a large-area TiO_2 can be prepared by the simple doctor blade method, nc- TiO_2 electrode constitutes a good candidate for EC applications, taking advantage of its excellent properties in terms of chemical stability.

1.2. Thermochromic windows

Thermochromic coatings are the materials that can change the optical properties (transmission, reflection and absorption) under the action of temperature. One of the most prospective thermochromic materials is vanadium dioxide (VO_2), because VO_2 films can be used for many applications, such as sensors [16], smart thermochromic windows [17] and thermal glazing. Many previous works have focused onto subject of V-based compounds of different structures like V_2O_5 , VO_2 , LiV_3O_8 aiming at searching for applications. To prepare the thin vanadium oxides films one can use different techniques, for instance, vacuum evaporation using boat resistance, RF-sputtering, CVD, etc. We have also used the electron beam technique for depositing VO_2 films [18]. Recently, thermochromic VO_2 films on stainless steel substrate were deposited by DC- reactive magnetron sputtering. The authors [19] showed that the semiconductor-to-metal phase transition (SMPT) temperature can be reduced simply by selecting the annealing temperature that induces local nonstoichiometry; a SMPT temperature as low as 42.7°C was obtained by annealing the film at about 440°C . With the aim to improve the efficiency of the thermochromic performance we prepare nanostructured VO_2 films by RF-sputtering followed by post thermal annealing.

Fig. 3 shows the XRD of the samples obtained by RF-sputtering and followed by post thermal treatment for two kinds of targets: one is the VO_2 and the other is V_2O_3 . It is seen that although the stoichiometry of VO_2 target is matched to the vanadium dioxide, the sputtering process resulted in decomposition, consequently in the film there was observed majority of V_6O_{11} and minority of the VO_2 (this is confirmed by the much stronger intensities of the XRD peaks of V_6O_{11} , see patterns A, Fig. 3). Whereas, by using a V_2O_3 target, the annealed film exhibited a single phase of VO_2 film with seven peaks corresponding diffraction (hkl) planes: $(\bar{1}11)$, (011) , $(\bar{1}02)$, $(\bar{2}11)$, (020) , (220) and (022) (see the patterns B, Fig. 3). Thus, to deposit VO_2 films V_2O_3 targets are more suitable than VO_2 targets. Further, all the samples used for the study were deposited by RF-sputtering from the V_2O_3 target, followed by annealing in low pressure of gaseous oxygen.

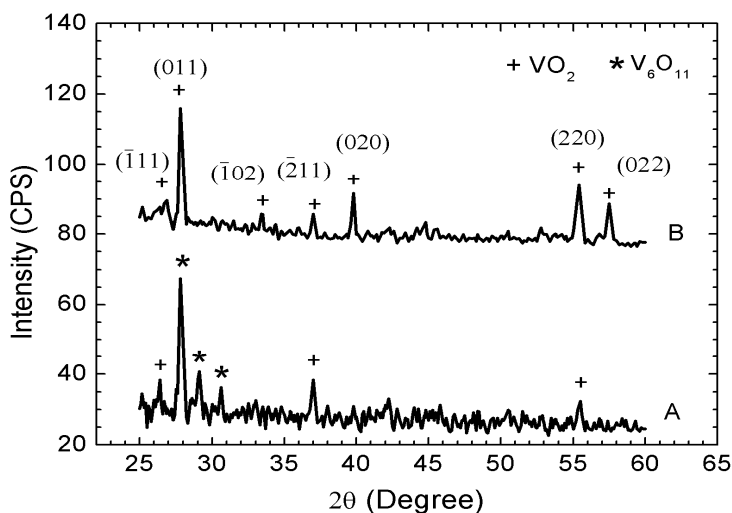


Fig. 3. XRD patterns of vanadium oxide films deposited by RF-sputtering followed by annealing. “A” patterns is of the film sputtered from VO_2 target and “B” patterns – from V_2O_3 target.

From XRD patterns, grains size was found to be of ~ 200 nm. This is in a good agreement with the data obtained by SEM for the average size of grains. The thickness of the annealed film (d) was measured from a FE-SEM scanned at a cross section of the film by point-to-point marking technique, as shown in Fig. 4a. The average value of the thickness was evaluated as about 240 nm. As-sputtered film was fine and amorphous, during annealing the film was recrystallized with submicro-structured grains of a size about 200 - 250 nm (Fig. 4b). From the SEM picture, one can observe dark holes between the grains that reflect the glass-substrate surface. This proves the local shrinkage of the film during re-crystallization process and these holes have the depth as large as the grains size. Thus one can suggest that the films have a single-layer submicro-structured material of vanadium dioxide.

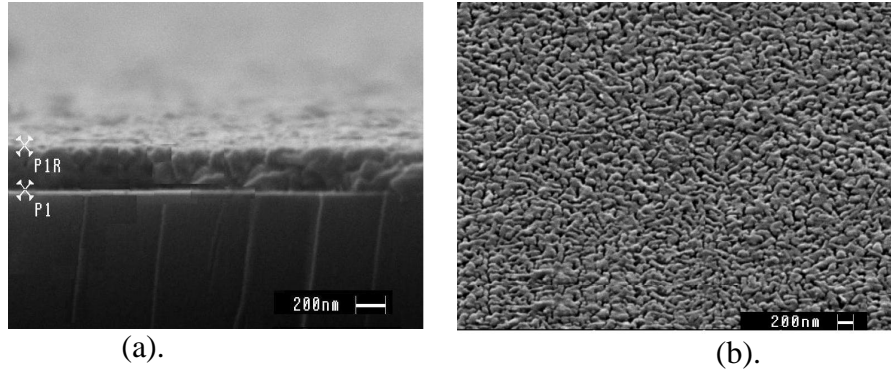


Fig. 4. SEM micrographs of a cross section of the annealed film (a) and surface morphology of the film. This clearly shows the submicro-structured grains of VO_2 which were crystallized during the annealing. The thickness $d = 240$ nm.

The temperature dependence of the resistivity of both the as-deposited and annealed films is plotted in Fig. 5. From XRD analysis it has been known that as-deposited films exhibited vanadium-rich and amorphous films. Typical resistivity of such a thin film consists of $7\div 15 \Omega \times \text{cm}$. Since the temperature dependence of resistivities obeys a law of electrical property of metal oxides, the resistivity decreases with increasing of temperature, one can expect that the lack of oxygen atoms in the vanadium oxide compounds is not so much, that the films can be recrystallized in low vacuum maintaining by gaseous oxygen flow. Indeed, during annealing at 450°C in an oxygen pressure of 1.33 Pa the amorphous film has transformed into a crystalline film. For the annealed film, the temperature dependence of resistivity in a range from room temperature to 100°C is shown interestingly. There was observed an critical temperature, where occurred an abrupt change of the resistivity. This temperature is called “temperature of SMPT” (τ_c). Bellow τ_c the ρ -T curve exhibits the property of a semiconducting phase (SP) with an activation energy as large as 0.023 eV. SP is also called “low-T phase”. Above τ_c this curve seems to be similar to that of a metallic phase (MP) which is called “high-T phase”. The ratio of resistivities ($\rho_{\text{sp}}/\rho_{\text{mp}}$) of the high-T and low-T phases is about 3 order in magnitude that can be comparative to $\rho_{\text{sp}}/\rho_{\text{mp}}$ of a bulk VO_2 crystal. Besides, τ_c of the submicro-structured film is observed at 64°C (Fig. 3) which is about 3°C lower than that of a standard bulk VO_2 which possesses $\tau_c \sim 67^\circ\text{C}$. This can be attributed to lowering of the free energy of the submicro-structured films in comparison with that of the bulk sample.

Overcoming the τ_c , nano-structured VO_2 films also possess an abrupt change in the transmittance spectra (Fig. 6). The largest difference between transmittances of the high-T phase and the low-T phase was observed at an IR-wavelength of 2500 nm. However, at $\lambda = 1550$ nm – the wavelength of popular fiber-optic lasers – the difference reaches a value as high as 25% (namely $T_{\text{SP}} - T_{\text{MP}} = 55\% - 30\%$, see Fig. 6). This difference is explained as follows. At temperature higher than τ_c when the VO_2 film completely transformed into the metallic phase with a tetragonal crystalline lattice (whereas semiconducting phase of VO_2 has a monoclinic

lattice). In the high-T phase the electronic structure of VO₂ is strongly changed: Vd and Op orbitals are overlapped resulting in disappearance of the band gap which is existent in the low-T phase of VO₂.

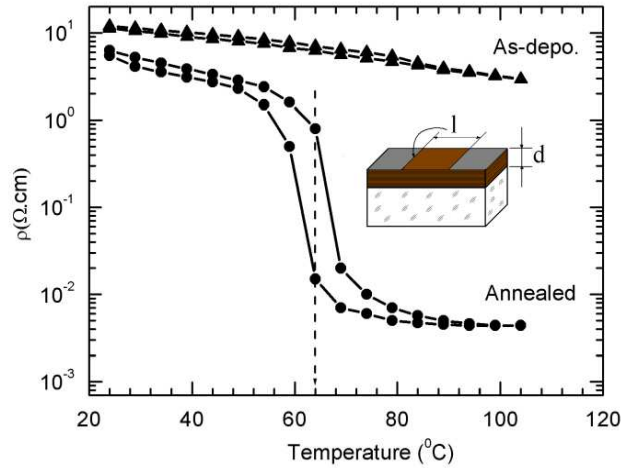


Fig. 5. The temperature dependence of the resistivity of as-deposited film (top) and annealed film (bottom loop).

Thus the density of quasi-free electrons in metallic phase increases, consequently the resistivity of the film is lowering and IR-reflectance – increasing, that is why the transmittance decreased. This behavior of VO₂ when overcoming τ_c suggests a potential application in production of thermo-optical sensors used for monitoring accidental change of temperature in environment, especially for toxic chemicals and petrol storages where the remote optical control of temperature should be utilized.

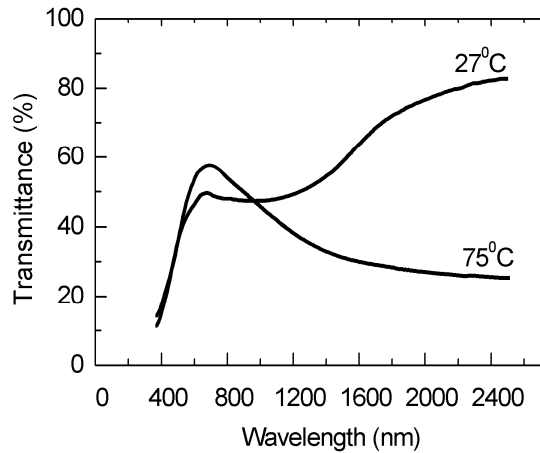


Fig. 6. Transmittance spectra of VO₂ film recorded at temperature lower τ_c (top curve) and at temperature higher τ_c (bottom curve).

Thus, for TE-smart windows, nano-structured vanadium dioxide films have been prepared by RF-sputtering with use of a V₂O₃ ceramic target and followed by thermal annealing in an oxygen pressure of 1.33 Pa. SEM and XRD structural analysis showed that the VO₂ film were crystallized in a single layer with submicro-structured grains of 200 to 250 nm in size. The films have temperature of the semiconductor-to-metal phase transition $\tau_c = 64^\circ\text{C}$ which is slightly smaller than that of the bulk crystals of VO₂. At temperatures higher τ_c the resistivity of the films decreased three orders in magnitude and the transmittance (at $\lambda = 1550$ nm) lowered from 55% to a value as low as 30%. This suggests a practical application in production of a thermo-optical sensor that can be used in monitoring temperature change of liquid and/or toxic chemicals in storages.

II. Solid-state lighting

It is known that the solid-state lighting (SSL) is based on lighting from light emitting diodes (LEDs) rather than conventional incandescent and fluorescent lights. Since SSL produces visible light while giving off less heat and reducing energy loss, it has potential applications in both the life and the lighting industrial technology. This technology holds promise for lower energy consumption and reduced maintenance [20,21].

There are three methods to generate white light by LEDs such as Red + Green + Blue LEDs, UV LED + RGB phosphor and Blue LED + Yellow phosphor (Fig. 7). Each method has own advantages as well disadvantages. By the first method one can make white light by combining three LEDs with red, green and blue colors. It is a better choice to produce white light with long term, high efficiency, dynamic tuning of color temperature, excellent color rendering and very large color Gamut. However, this method has also limitations; for example, the color feedback requires accounting for LED degradation with temperature and time, the color mixing and the yellow green gap. In the second method the white light can be done by using UV-LEDs for the excitation of the RGB phosphor. The advantages of this method are following, the white point can be determined by a single phosphor, the color rendering is reasonable, and the phosphor possesses an excellent temperature stability. But the disadvantage of this method can be also mentioned such as a low-efficient blue LED pumped phosphor, different angle color uniformity, and the need of UV exposure packaging and the lack of the all-temperature stability of phosphor. In the last method the white light is obtained by combining the blue LED with yellow phosphor. This method is simple and useful for the generation of the white light and has the following advantages like single yellow phosphor versions available today, decent color rendering, and temperature stability of phosphor. However, this method also faces to many challenges such as temperature stability of phosphor is not available in all colors, color uniformity with angle. Besides the advantages and challenges, this method has many disadvantages such as limits on efficiency due to phosphor conversion efficiency, Stokes shift, self absorption, etc.

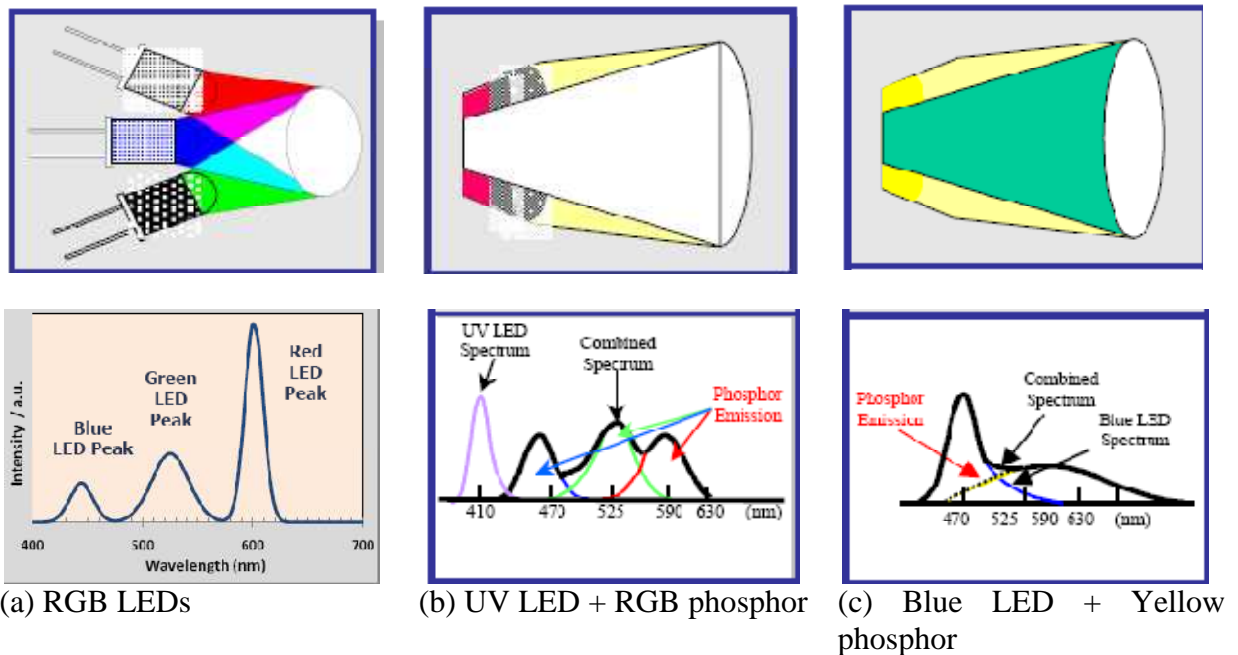


Fig. 7. Three methods used for producing the white light LEDs: (a) - Red + Green + Blue LEDs, (b) - UV LED + RGB phosphor and (c) - Blue LED + Yellow phosphor.

The composites were made from the nanostructure Ce-doped yttrium aluminum garnet (YAG:Ce) and conjugate polymer of (Poly[2-methoxy-5-(2'-ethyl-hexyloxy)-1,4- phenylene vinylene] (MEH-PPV). The green YAG:Ce (G-YAG) nanopowder was prepared by low-temperature sol-gel method. The pure MEH-PPV powder was prepared by dissolving in

toluene solvent with a ratio of 1 mg of MEH-PPV powder in 2 ml toluene. The G-YAG nanopowder in the MEH-PPV solution was mixed in a liquid transparent epoxy. The last was then coated onto the glass substrate for the optical characterization and onto the blue LEDs chip for the investigation of electroluminescence performance, respectively. The blue InGaN-LED chip used in this research has the peak wavelength at 455 nm and 1W power blue LED (with the die size around 1100 μm x 1100 μm , as can be seen elsewhere [22]). The green phosphor and MEH-PPV polymer hybrid composite were dropped onto the surface area between the top of the LED chip to convert a part of blue light into green and red lights.

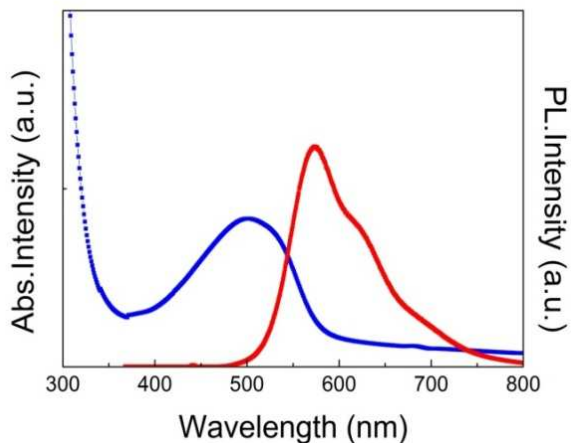


Fig. 8. Absorption and Photoluminescence spectra of MEH-PPV film.

The absorption and photoluminescent spectra of MEH-PPV films are showed in the Fig. 8. From this figure one can notice that the MEH-PPV film has an absorption peak a 490 nm and two emission peaks at around 590 nm and 620 nm. This proves that for the excitation of MEH-PPV polymer an InGaN blue LED chip with 460 nm peak of the emission is quite efficient. Indeed, the realization of using the hybrid composite to make a WLED gave a total emission spectrum as demonstrated in Fig. 9.

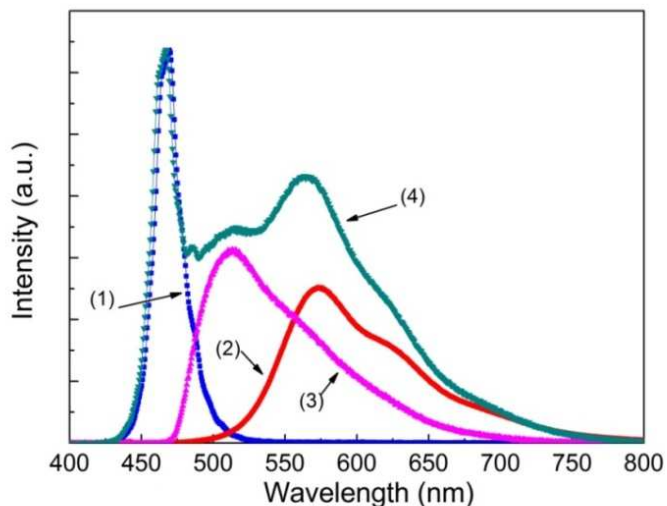


Fig. 9. Emission spectra of components of WLEDs made from nanocomposite: Blue LED (1), MEH-PPV (2), G-YAG:Ce nanopowder (3) and the total spectrum of the Blue LED, G-YAG:Ce and MEH-PPV (4).

From photoluminescence spectra of G-YAG:Ce and MEH-PPV polymer one can expect that the mixed light emitted from three components as blue the LED chip, G-YAG:Ce and MEH-PPV polymer exhibits the white light with a broad band luminescent spectrum and a high CRI. In particular, with the use of G-YAG and MEH-PPV hybrid composite, the spectral region is enhanced around the wavelength of 521 nm that is due to the contribution of the emission of the G-YAG. The increase of the intensity of the 521 nm peak enables the color rendering index increased. Such performance of the WLED was more revealable when the WLED was made from coating a nanocomposite with a weight ratio of 2/1 of G-YAG / MEH-PPV powders on a blue LED chip. The emission spectrum of the WLED put under a supply power of 3.5 V is plotted in Fig. 10, clearly showing better electroluminescence spectra of the white light.

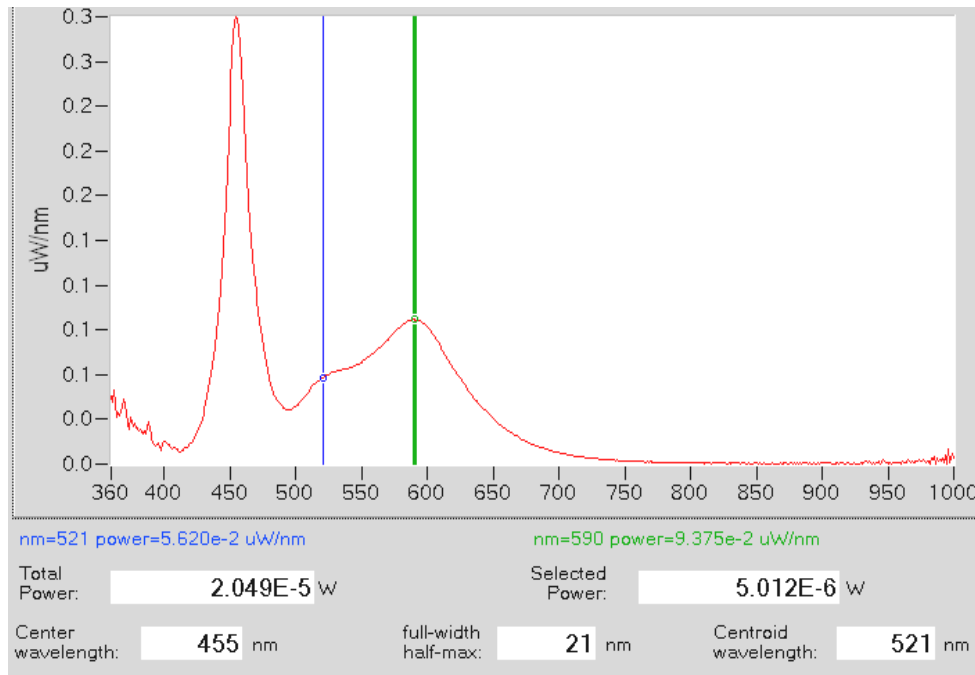


Fig. 10. Emission spectra of WLEDs made from by coating G-YAG and MEH-PPV hybrid composite onto InGaN blue chip.

To determine the CRI of the WLED made from a 300 μm - thick hybrid nanocomposite film, the device was put on the integrating sphere equipped with a calibrated spectrophotometer LCS-100 and supplied with a 3.5 V voltage and 200 mA forward current. The obtained results from the measurements for the colour coordinates at $x = 0.2986$ and $y = 0.2620$ is shown in Fig. 6. One can notice that the white light region is located inside the ellipse with the centre at $x = 0.33$ and $y = 0.33$. It is seen that for the WLED, the CRI was found to be as high as $R_a = 84.36$.

Thus, we have the fabricated and characterized so called WLED for solid-state lighting. Photo- and electroluminescent spectra of the hybrid nanocomposite of the green YAG:Ce and MEH-PPV conjugate polymer showed that a novel white LED composed of G-YAG:Ce and MEH-PPV polymer and InGaN chip giving a highly-efficient performance can be made. This WLED exhibits a broad band emission spectrum from blue light to red wavelengths, that is more adapted to the human eye sensitivity. The hybrid nanocomposite based WLEDs provided the white light with a CIE-1931 coordinate of $x = 0.2986$, $y = 0.2620$ and a colour rendering index $R_a = 84.36$. The obtained results suggest a potential application of nanocomposite based WLEDs in efficient solid-state lighting, consequently in the valuable contribution to the energy sustainability.

III. Organic Solar Cells (OSC)

Recently, solar cells based on organic materials are increasingly interesting because of their possibility to reduce the fabrication cost [23,24]. Organic solar cells (OSCs) should have the following features: a strong light absorption over the whole solar spectrum; an appropriate energetic distance between the highest occupied molecular orbital (HOMO) and the lowest occupied molecular orbital (LUMO) of polymer to form a high open circuit voltage; a high and balanced electron and hole mobility in the polymer layer. When sufficient energy is applied to a semiconducting polymer, electrons from the HOMO level (valence band) are excited to the LUMO level (conduction band). This excitation process leaves holes in the valence band, and thus creates “electron-hole-pairs” (EHPs). When these EHPs are in intimate contact (i.e., the electrons and holes have not dissociated) they are termed “excitons”. To develop viable devices such as OSCs there are two main approaches that have been developed [25]: (i) the donor–acceptor bilayer, commonly achieved by vacuum deposition of molecular components, and (ii) the so-called bulk heterojunction (BHJ), consisting of a bicontinuous composite of donor and acceptor phases. Among numerous electrically conducting polymers, poly[2-methoxy-5-(2-ethylhexyloxy)-1,4-phenylenevinylene] (MEH-PPV) with an energy bandgap of 2.2 eV [7]) and poly(3-hexylthiophene) (P3HT) are mostly used for organic electronic devices such as light emitting diodes (OLED) and OSCs, respectively. The BHJ solar cells based on poly(3-hexylthiophene) (P3HT) with an energy bandgap of 1.9 eV and the fullerene derivative [6,6]-phenyl-C61-butyric acid methyl ester (PCBM) - that are currently considered to be the ideal acceptors for OSC –have been widely investigated. PCBM have an energetically deep-lying LUMO, which endows the molecule with a very high electron affinity relative to the numerous potential organic donors like P3HT. However, the efficiency of an organic solar cell until now is considerably low; this is usually attributed to the strong decay of the excitons which are generated in the donors/acceptors junctions owing to the illumination of solar radiation. The excitons decay can be diminished by the creation of either appropriate heterojunctions or nanocomposite layers. This results in the charge separation, i. e. generated electrons and holes move in opposite directions, and consequently the luminous quenching occurs. Thus by characterization of the quenching behavior of polymeric composite materials, one can have preliminary evaluations on the photoelectrical conversion efficiency of the materials used for OSCs.

To compare the photoactive properties of MEH-PPV and P3HT nanocomposites, two types of OSCs based on MEH-PPV and P3HT were prepared, using ITO with a sheet resistance of 10Ω . The ITO-coated glass substrates used for spincoating nanocomposite films were ultrasonically cleaned in distilled water, followed by cleaning in ethanol and acetone. To deposit the composite layers onto ITO, MEH-PPV and P3HT solutions were prepared by dissolving MEH-PPV and P3HT powders, respectively in xylene and chlorobenzene as follows: 10 mg of MEH-PPV in 1 ml of xylene and 8 mg of P3HT in 1 ml of chlorobenzene. Then, TiO_2 nanoparticles with 5 nm and 15 nm in size were embedded, respectively in MEH-PPV and P3HT solutions according to a same weight ratio $\text{TiO}_2/\text{polymer}$ of 0.05 (namely 5 wt. %), further referred to as MTC and PTC. To obtain a homogenous dispersion of TiO_2 in polymers, the solutions were mixed for 8 hours by using magnetic stirring. These liquid composites were then used for spin-coating. The conditions for spin-coating are as follows: a delay time of 120 s, a rest time of 30s, a spin speed of 1500 rpm, and an acceleration of 500 rpm, and finally a drying time of 2 min. The films used for photoluminescence (PL) characterization were spin-coated onto glass pieces with $1.2\text{ cm} \times 1.2\text{ cm}$ in size. For the acceptor layer, a 50 nm-thick PCBM layer was then spin-coated onto the nanocomposite layers. To dry the films, the samples were put in a flow of dried gaseous nitrogen for 12 hours. Then a 70 nm-thick Al-electrode on the top was thermally evaporated in a vacuum of $1.33 \times 10^{-3}\text{ Pa}$, using a mask with windows of $4\text{ mm} \times 5\text{ mm}$ in size. Therefore, the active area of a cell is 0.20 cm^2 . By this way, two type of organic solar cells (OSC) which have structure of Al/PCBM/MTC/Al and Al/PCBM/PTC/Al were prepared, as shown in **Fig. 11**.

Absorption spectra of the samples were carried-out on a Jasco V-570 UV-Vis-Nir spectrometer. Quenching effect of the nanocomposite layers was studied by photoluminescence spectra on a FLuoroMax-4 spectrofluorometer, using radiation of Xe-lamp for excitation. The performance of the OSCs was carried-out on an AutoLab-Potentiostat PGS-12 electrochemical unit with an illumination power of 56 mW/cm² taken from "Sol 1A" Newport source which provides an energy spectrum similar to the solar one.

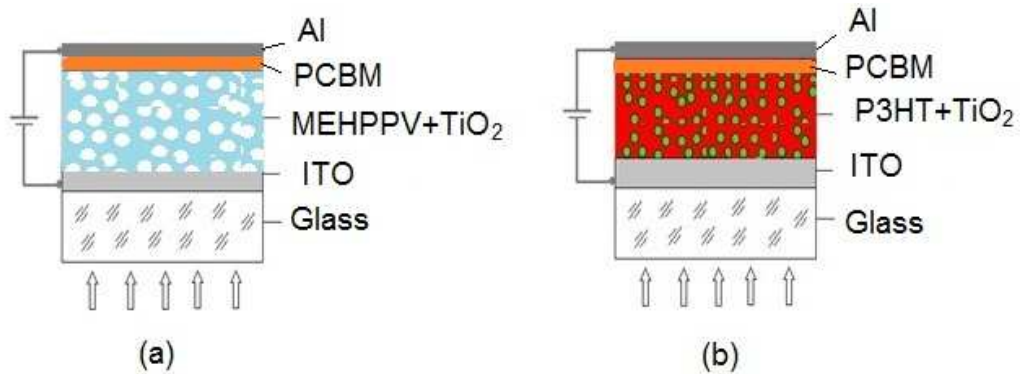


Fig. 11. Schematic drawing of OSCs based on nanocomposite of MEH-PPV+TiO₂ (a) and P3HT+TiO₂ (b). Thickness of the MTC and PTC layers is ~ 120 nm, PCBM layer – 50 nm and Al-electrode - 70 nm.

To find out a wavelength range for excitation, absorption spectra in the UV-Vis range for the polymers were recorded. From UV-Vis spectra it has been known that the absorption peak was found at ~ 510 nm for MEH-PPV, whereas P3HT have two peaks at 495 nm and 528 nm and one shoulder at 573 nm. These three bands can be attributed to the π - π^* transition. These values were similar to the ones that have been reported for P3HT [10]. Polymeric composites (with the presence of nc-TiO₂ particles) have almost the same absorption spectra, except one peak in ultra-violet (360 nm) of TiO₂. Fig. 12 shows the PL spectra of pure polymers and the polymer/nc-TiO₂ films, all the measurements were carried-out at room temperature. For both two polymeric composites (namely MTC and PTC) the luminescence quenching of samples was observed at red wavelengths. For pure polymeric samples, the photoemission has a broad peak at 640 nm (for MEH-PPV) and 720 nm (for P3HT). For PTC sample that contains numerous P3HT/nc-TiO₂ heterojunctions, a blue shift of the photoemission peak of ~ 25 nm was observed, whereas for the MTC, a negligible shift appeared. This blue shift is similar to the one for the hybrid sample of poly(para-phenylene vinylene) (PPV)/nc-SiO₂ and was explained by a reduction in the polymer conjugation chain length, when nanoparticles of SiO₂ were embedded in the polymer [26]. In our experiments, the polymer/nc-TiO₂ polymer was partially broken by the TiO₂ nanoparticles.

To compare the quenching between MTC and PTC samples one can introduce a relative quenching coefficient (χ) that is calculated by following equation.

$$\chi = (I_p - I_c) / I_p \quad (2)$$

where I_p and I_c are the intensities of the PL peak of polymers and composites, respectively. From Fig. 3 and by applying Eq. (2), χ of MTC and PTC samples was found to be of 19.2% and 45.5%, respectively. The result of the calculation shows that the quenching coefficient of PTC sample is more than two times larger than that of the MTC sample. Note that the size of nc-TiO₂ particles embedded in P3HT is three times larger than the size of nc-TiO₂ embedded in MEH-PPV. Thus, the size of the quencher TiO₂ nanoparticles influences the photoluminescence quenching of the polymeric composites. This matches the reported result on poly(*N*-vinylcarbazole)(PVK) polymer containing Au nanoparticles. Thipperudrappa et al. showed that the fractional intensity I_p / I_c is given by the product of both static and dynamic quenching [27]. The authors also demonstrated that instantaneous or static quenching occurs if

the quencher substances are very near to, or in contact with fluorescent molecules at the moment of its excitation. In other words, the electron-hole pairs generated at the heterojunctions (i.e. polymer/nc-TiO₂ interfaces) are not recombined; they are separated from each other, resulting in the luminous quenching of polymeric composite thin films. This is a specific property that is desired for designing a simple, but prospective organic solar cell. The fact that the quenching is closely involved to the charge separation proves that the luminous quenching can be considered as a useful factor for choosing a combination of conducting polymers and inorganic nanoparticles used for OSCs fabrication.

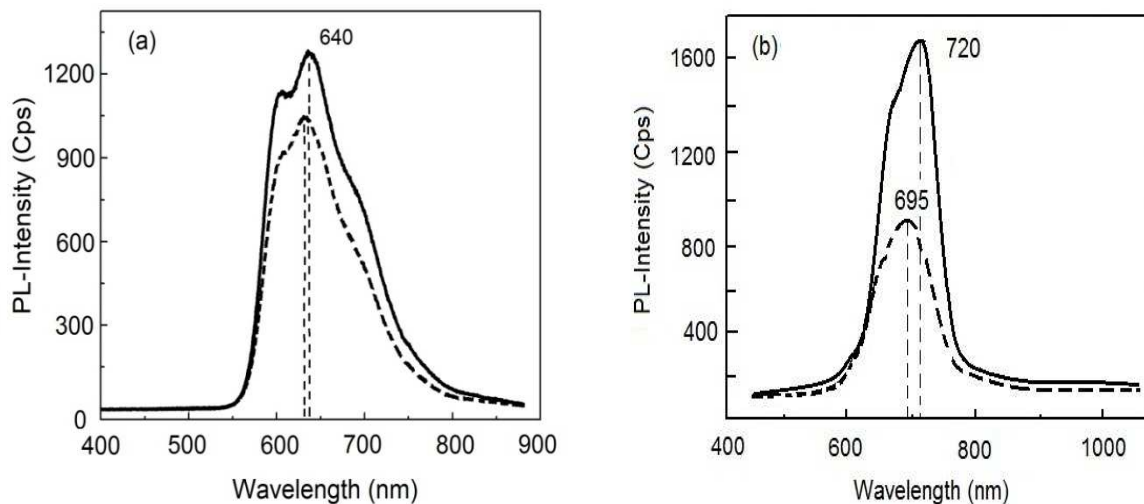


Fig. 12. (a): PL spectra of MEH-PPV and MEH-PPV/nc-TiO₂ (5 nm); (b): P3HT and P3HT/nc-TiO₂ (15 nm).

In addition, the difference in quenching properties of the MTC and PTC samples can be explained by the use of the energy bandgap structures of the heterojunctions (Fig. 13). Herein, the energy values showed in the diagram are reported as absolute values relative to a vacuum level of MEH-PPV [8] and P3HT [14].

The energy bandgap (E_g) of P3HT, MEH-PPV and TiO₂ is 1.9, 2.2 and 3.3 eV, respectively. The difference between conducting band level of TiO₂ and LUMO level of MEH-PPV and P3HT is $\Delta E_1 = 1.3$ eV and $\Delta E_2 = 0.9$ eV, respectively (Fig. 4). When polymers were excited by a beam with energy larger than E_g of polymers, generated electrons jumped from the HOMO to the LUMO and in the HOMO holes appeared. Since the conducting band level in TiO₂ is lower than the LUMO level, electrons diffused to the conductor band of TiO₂. On the contrary, holes moved from the valence band of TiO₂ to the HOMO band of polymers, resulting in the charge separation. Since ΔE_2 is much smaller than ΔE_1 , generated electrons move more easily to nc-TiO₂. If the difference in energy between the conducting band level of TiO₂ and LUMO level of polymer is large like ΔE_1 , one can use electron conducting buffer between them, similarly to ZnO that was used as buffer material sandwiched between ITO and PCBM, as reported in [28].

As mentioned above, OSCs based on MTC (OSC-1) and PTC (OSC-2) thin layers were made for a comparison of their performances. Characterization of the device parameters such as open voltage (V_{OC}), short cut current density (J_{SC}) and fill factor (FF) was carried out with the Auto-Lab. potentiostat using cyclic voltammetry (CV) measurements in both the dark and illumination.

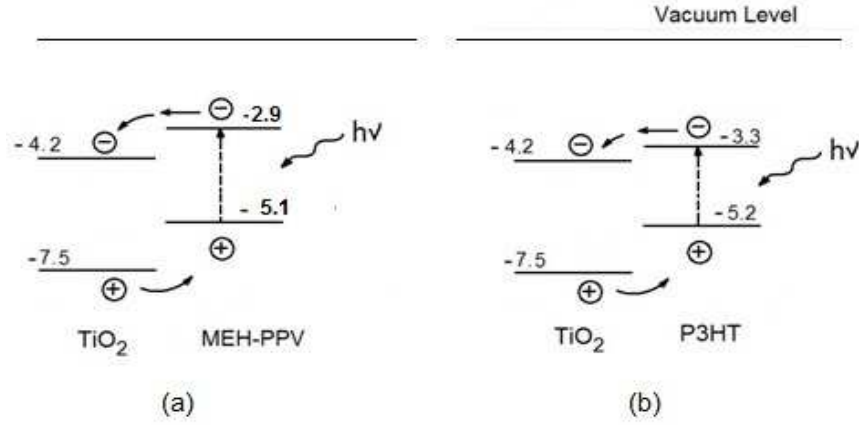


Fig. 13. Band structure diagram illustrating the HOMO and LUMO energies of MEH-PPV (a) and P3HT (b) relative to the band structure of TiO₂.

In this case CV curves shown in Fig. 14 just revealed current-voltage (I-V) characteristics of two devices OSC-1 and OSC-2. In this figure the light-gray rectangle illustrates a fill factor that is determined by charge carriers reaching the electrodes, when the built-in field is lowered toward the open circuit voltage. In fact, there is a competition between charge carrier recombination and transport. So that, FF can be determined by:

$$FF = \frac{(J \times V)_{max}}{J_{sc} \times V_{oc}} \quad (3)$$

where $(J \times V)_{max}$ is the rectangle having the largest area. Then the photoelectrical conversion efficiency (PCE) can be determined by:

$$PCE = \frac{FF \times J_{sc} \times V_{oc}}{P_{in}}, \quad (4)$$

where P_{in} is the density of the illuminating power, in mW/cm^2 . In our experiments P_{in} was taken at a value of $56 mW/cm^2$.

By applying formulas (2) and (3), FFs of OSC-1 and OSC-2 were calculated and equal to 0.53 and 0.64, respectively. And PCE of OSC-1 and OSC-2 was found to be of 0.17% and 0.45%, respectively. It means that PCE of OSC-2 is more than two times larger than that of OSC-1.

The fact that the fill factor of OSC-2 is larger than that of OSC-1 proves that in comparison with MEH-PPV, conducting polymer P3HT is a better matrix where nc-TiO₂ nanoparticles are more tightly surrounded. This is because during the spinning process in the spin-coating technique, the TiO₂ nanoparticles can adhere by a strong electrostatic force to the polymer and between themselves, and capillary forces can then draw the P3HT solution around the inorganic nanoparticles into cavities without opening up pinholes through the device.

Thus, for OSCs, nanocomposite materials containing heterojunctions of MEH-PPV+ nc-TiO₂ and P3HT+nc-TiO₂ were prepared by spincoating MEH-PPV and P3HT on ITO electrodes. Luminous quenching was observed for both polymeric composites, but the quenching coefficient of P3HT+nc-TiO₂ is much larger than that of MEH-PPV+ nc-TiO₂. The results obtained on the relationship of PL quenching and photoelectrical efficiency of the OSC showed that the quenching coefficient can be seen as a useful criterion for choosing appropriate polymers and inorganic nanoparticles being used for the further preparation of OSCs. Under an illumination of solar energy of $56 mW/cm^2$, photoelectrical efficiency P3HT+nc-TiO₂ based OSC reached a value of 0.45%.

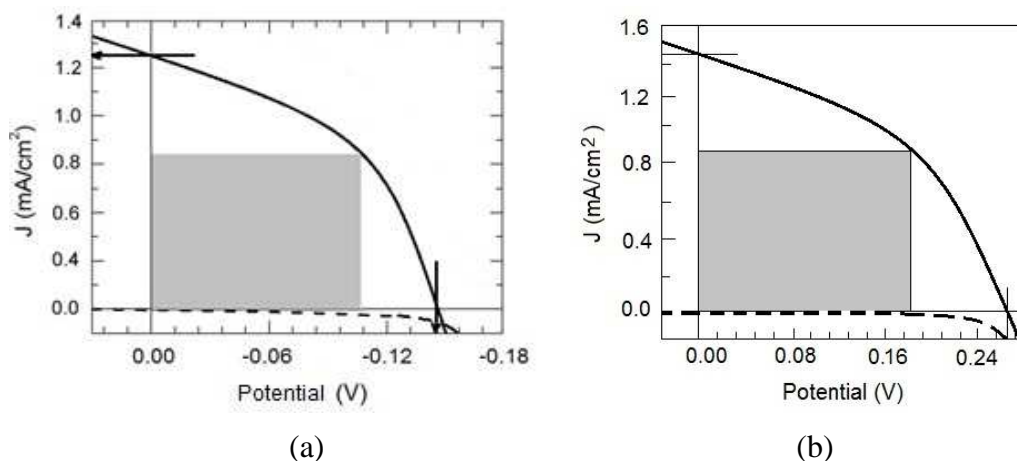


Fig. 14. Current-voltage characteristics of OSC-1(a): $P_{in} = 56 \text{ mW/cm}^2$, $V_{oc} = 0.14 \text{ V}$, $J_{sc} = 1.24 \text{ mA/cm}^2$, $FF = 0.53$, $PCE = 0.17\%$ and OSC-2 (b): $P_{in} = 56 \text{ mW/cm}^2$, $V_{oc} = 0.243 \text{ V}$, $J_{sc} = 1.43 \text{ mA/cm}^2$, $FF = 0.64$, $PCE = 0.45 \%$.

Conclusion

Some projects on non-conventional energy or *Green Energy*. In this overview report we have shown main research results concerning to solar energy, including only there R-D groupes: The first, research and application of how to use solar radiation most efficiently, so called "Energy-Efficient Windows"; the second, research and produce of solid-state lighting sources - the most ennergy-efficient lighting lamps; and the last, research of new type of solar cells, such as Organic Solar Cells (OSC). We presented also technology and characterization of nanostructured materials used for improvement of the performance of the devices, such as TiO_2 and VO_2 for electrochromic and thermochromic (smart) windows; hybrid nanocomposite of G-YAG:Ce and MEH-PPV conjugate polymer used for solid-state lighting and nanocomposite materials containing heterojunctions of P3HT+nc- TiO_2 used for organic solar cells.

Acknowledgments

This overview report was taken from projects supported by the MOST of Vietnam through the Project on Fundamental Scientific Research for Applications and Vietnam National Foundation for Science and Technology Development (NAFOSTED).

Infrastructure and equipment provided for YAG:Ce synthesis, XRD patterns, NST treatments were made possible in the VNU project on "Nanotechnology and Application" in the period 2010-2013 supported by the Vietnamese Government.

References

- [1] C.G. Granqvist, Handbook of Inorganic Electrochromic Materials, Elsevier, Amsterdam, The Netherlands, 1995.
- [2] A. Azens, G. Gustavsson, R. Karmhag, C.G. Granqvist, Electrochromic devices on polyester foil, *Solid State Ionics* 165 (2003) 1–5.
- [3] E. Avendaño, L. Berggren, G.A. Niklasson, C.G. Granqvist, A. Azens, Electro-chromic materials and devices: brief survey and new data on optical absorption in tungsten oxide and nickel oxidefilms, *Thin Solid Films* 496 (2006) 30–36.
- [4] T. Seike, J. Nagai, Electrochromism of 3d transition metal oxides, *Solar Energy Materials* 22 (1991) 107–117.
- [5] Y.-H. Ye, J.-Y. Zhang, P.-F. Gu, X. Liu, J.-F. Tang, Electrochromism of titanium oxide thinfilms, *Thin Solid Films* 298 (1997) 197–199.

- [6] S.F. Cogan, E.J. Anderson, T.D. Plante, R.D. Rauh, Materials and devices in electrochromic window development, *Proceedings of SPIE—The International Society for Optical Engineering* 562 (1985) 23–31.
- [7] A. Gutarra, A. Azens, B. Stjerna, C.G. Granqvist, Electrochromism of sputtered fluorinated titanium oxide thinfilms, *Applied Physics Letters* 64 (1994) 1604–1606.
- [8] M. Kitao, Y. Oshima, K. Urabe, Preparation and electrochromism of RF-sputtered TiO₂films, *Japanese Journal of Applied Physics* 36 (1997) 4423–4426.
- [9] K.D. Lee, Optical and electrochromic properties of TiO₂ films prepared by using RF-magnetron sputter deposition, *Journal of the Korean Physical Society* 52 (2008) 1070–1076.
- [10] T.J. Richardson, M.D. Rubin, Liquid phase deposition of electrochromic thin films, *Electrochimica Acta* 46 (2001) 2119–2123.
- [11] K. Lee, D. Kim, S. Berger, R. Kirchgeorg, P. Schmuki, Anodically formed mesoporous TiO₂ electrodes for high electrochromic contrast, *J. Materials Chemistry* 22 (2012) 9821–9825.
- [12] N.N. Dinh, N.M. Quyen, D.N. Chung, M. Zikova, V.-V. Truong, Highly efficient electrochromic performance of nanostructured TiO₂ made by doctor blade technique, *Solar Energy Materials and Solar Cells* 95 (2011) 618–623.
- [13] N.N. Dinh, D.H. Ninh, T.T. Thao, V.-V. Truong, Mixed nanostructured Ti–W oxidesfilms for efficient electrochromic windows, *Journal of Nanomaterials* 781236 (2012) 1–7.
- [14] P. Delichere, P. Falaras, A. Hugot-Le Goff, WO₃ anodic films in organic medium for electrochromic display devices, *Solar Energy Materials* 19 (1989) 323 – 333.
- [15] N. N. Dinh, N. Th. T. Oanh, P. D. Long, M. C. Bernard, A. Hugot-Le Goff, Electrochromic properties of TiO₂ anatase thin films prepared by dipping sol-gel method, *Thin Solid Films* 423 (2003) 70 – 76.
- [16] C. M. Lambert, *Solar Energy Mater*, Vol. 11 (1984) p.1
- [17] C. M. Lampert and C.G.Granqvist, eds, in “Large-area Chromogenics: Materials and Devices for Transmittance Control”, Vol. 154 (SPIE Optical Engineering Press, Bellingham, 1990).
- [18] Do Hong Thanh, Phan Van Anh and Nguyen Nang Dinh, *Communications in Physics* 10 (2000) p. 143
- [19]. Z. Zhang, Y. Gao, Z. Chen, J. Du, C. Cao, L. Kang, H. Luo, *Langmuir*, 2010, 26 (13), pp 10738–10744.
- [20] J. Y. Tsao (Member, IEEE), M. E. Coltrin, M. H. Crawford (Member, IEEE), and J. A. Simmons, *Solid-State Lighting: An Integrated Human Factors, Technology and Economic Perspective*, *Proceedings of the IEEE* (2009).
- [21] Y. T. Lin, T. W. Zeng, W. Z. Lai, C. W. Chen, Y. Y. Lin, Y. S. Chang, W. F. Su, *Nanotechnology* 17 (2006) 5781.
- [22] L. Chen, C. C. Lin, C. W. Yeh, R. S. Liu, Light Converting Inorganic Phosphors for White Light-Emitting Diodes, *Materials* 3 (2010) 2172-2195.
- [23] C. J. Brabec, N. S. Sariciftci, J. C. Hummenmen. Plastic solar cell. *Adv. Funct. Mater.* 11 (2001) 15.
- [24] H. Hoppe, N. S. Sariciftci, *J. Mater. Research* 19/7 (2004) 1724.
- [25] B. C. Thompson, J. M. J. Frehet, *Angew. Chem. Int. Ed.* 47 (2008) 58.
- [26] S. H. Yang, T. P. Nguyen, P. Le Rendu, C. S. Hsu, *Composites Part A: Appl. Sci. Manufact.* 36 (2005) 509.
- [27] J. Thipperudrappa D. S. Biradar, and S. M. Hanagodimath, *J. Lumin.* 124 (2007) 45.
- [28] B. Freisinger, *Investigation of P3HT/PCBM Particle-Based Solar Cells*, Ph.D. dissertation, Mainz, FRG - 2013, p. 168.